Research Paper
Computational Methods for Differential Equations
http://cmde.tabrizu.ac.ir
Vol. *, No. *, *, pp. 1-15
DOI:10.22034/cmde.2025.68697.3347

A novel meshless technique based on generalized moving Kriging interpolation for Caputo–Hadamard time and Riesz space fractional reaction–diffusion equation

Ali Habibirad and Yadollah Ordokhani *

Department of Mathematics, Faculty of Mathematical Sciences, Alzahra University, Tehran, Iran.

Abstract

Considering the significant applications of fractional differential equations, their numerical solutions hold particular importance. Meshless methods have been employed by researchers for numerically solving these equations, which are often of integer order in the spatial dimension. However, the governing equation in this paper involves the spatial fractional derivative of the Riesz type and a singular Hadamard-type in spatial and time dimensions, respectively. Instead of deriving the global weak form of the problem, we utilize their weak form over local subdomains. In this study, for the first time, we calculate the Riesz-type fractional derivatives of the shape functions of the moving Kriging interpolation method and use them to discretize the reaction diffusion equation in the spatial dimension. The finite difference method is then applied to discretize the problem in the temporal dimension. We also conduct a convergence analysis, which demonstrates that the temporal order of the method is $O(\tau)$. To evaluate the accuracy and capability of the present scheme, three numerical examples are tested, and the results indicate high accuracy.

Keywords. Reaction diffusion equation, Moving Kriging technique, Caputo-Hadamard fractional derivative.
2010 Mathematics Subject Classification. 45A05, 47G10, 80M22.

Uncorrected

1. Introduction

Fractional differential equations have numerous applications in science and engineering. Due to the flexibility of these equations in modeling various phenomena, many researchers have turned their attention to studying this class of equations. Several definitions for fractional derivatives exist, for example Caputo derivative and the Riemann-Liouville derivative. The Hadamard fractional derivative is a type of fractional derivative that was first introduced and discussed by Hadamard in 1982 [16]. It has been established that the Hadamard derivative and fractional differential equations of the Hadamard type are valuable in mechanics, engineering, and other fields [2, 25]. In this work, we assume the following fractional reaction-diffusion models with singular kernels

$$\begin{aligned} &{}_{CH}D^{\beta}_{\gamma,t}u(\mathbf{s},t) - \Delta^{\alpha}u(\mathbf{s},t) + u(\mathbf{s},t) = f(\mathbf{s},t), \quad \mathbf{s}=(x,y)\in\Omega\subseteq[a,b]\times[c,d], \quad \gamma\le t\le T, \\ &u(\mathbf{s},\gamma) = u_1(\mathbf{s}), \qquad \text{Initial condition}, \\ &u(\mathbf{s},t) = u_2(\mathbf{s},t), \qquad \mathbf{s}\in\partial\Omega \quad \gamma\le t\le T, \quad \text{Boundary conditions}, \end{aligned} \tag{1.1}$$

in which u_1 and u_2 are known functions, $\alpha\in(1,2)$ and $\Delta^{\alpha}u(\mathbf{s},t) = (-\Delta_x)^{\alpha}u(\mathbf{s},t) + (-\Delta_y)^{\alpha}u(\mathbf{s},t)$, and this is the Laplacian for $\alpha = 2$. Also,

$$\begin{cases} (-\Delta_x)^{\alpha}u(\mathbf{s},t) = -\frac{1}{2\cos(\frac{\alpha\pi}{2})}[{}^{RL}_{a}D^{\alpha}_{x}u(\mathbf{s},t) + {}^{RL}_{x}D^{\alpha}_{b}u(\mathbf{s},t)], \\ (-\Delta_y)^{\alpha}u(\mathbf{s},t) = -\frac{1}{2\cos(\frac{\alpha\pi}{2})}[{}^{RL}_{c}D^{\alpha}_{y}u(\mathbf{s},t) + {}^{RL}_{y}D^{\alpha}_{d}u(\mathbf{s},t)], \end{cases} \qquad \alpha\neq 2k+1, \qquad k\in\mathbb{Z}, \tag{1.2}$$

Received: 17 August 2025; Accepted: 08 February 2026.
∗ Corresponding author. Email: ordokhani@alzahra.ac.ir.

T is the final time, ${}_a^{RL}D_x^{\alpha}$ is Riman Liuovill fractional derivative and $\partial\Omega$ is the boundary of global domain. Furthermore ${}_{CH}D_{\gamma,t}^{\beta}u(\mathbf{s},t)$ is Caputo–Hadamard derivative, defined as [27]:

$$ {}_{CH}D_{\gamma,t}^{\beta}u(t) = \frac{1}{\Gamma(\eta-\beta)}\int_{\gamma}^{t}\left(\log(\frac{t}{\zeta})\right)^{\eta-\beta-1}\delta^{\eta}u(\zeta)\frac{d\zeta}{\zeta}, \qquad 0<\gamma<t, \tag{1.3} $$

in which $\eta-1<\beta\leq\eta\in\mathbb{Z}^{+}$ and $\delta^{\eta}u(\zeta)=(\zeta\frac{d}{d\zeta})^{\eta}u(\zeta)$. From Eq. (1.3), for $\eta-1<\beta\leq\eta\in\mathbb{Z}^{+}$ we have

$$ {}_{CH}D_{\gamma,t}^{\beta}\left(\log(t/\gamma)\right)^{\kappa} = \begin{cases} \frac{k!}{\Gamma(\kappa-\beta+1)}\left(\log(t/\gamma)\right)^{\kappa-\beta}, & \kappa\geq\eta, \\ 0, & \kappa<\eta. \end{cases} \tag{1.4} $$

According to the applications of the reaction–diffusion equation, many methods were proposed to numerical solving of them. Authors of [3] developed a practical scheme based on operator splitting for solution of fractional reaction–diffusion equations. A finite difference scheme based on the Hermite formula, along with its stability and convergence properties, for solving the one-dimensional time-fractional diffusion equation is discussed in [27]. Kumar and his co authors introduced a higher-order finite difference scheme designed for solving generalized fractional diffusion equations in [23]. A technique of $L2$-type difference scheme achieving $3-\beta$ order time convergence, with second-order spatial discretization is shown in [19] for solving generalized time-fractional diffusion equation.

Meshless numerical methods offer significant capabilities for solving differential equations. Due to their flexibility, these methods have gained considerable popularity, attracting many researchers in the field. Among the meshless methods applied to the numerical solution of diffusion equations, the following approaches can be highlighted. The authors of [14] discussed a hybrid method based on the moving Kriging interpolation and finite difference technique for solving distributed order time-fractional reaction-diffusion equation. They used the $L2-1_{\sigma}$ method to approximate the solution of the fractional derivative discretization, and the unconditional stability and convergence rate of $O(\tau^2)$ for the time-discrete technique were illustrated. Dehghan and his colleagues [8] introduced an unconditionally stable and convergent meshless technique to numerical solving of time fractional diffusion-wave equation. The authors of [10] focus on a numerical simulation of an anomalous reaction-diffusion process in a two-dimensional space with a nonlinear source term. This study introduced an effective computational technique that combines a time integration scheme with the meshless local Petrov-Galerkin method to solve the problem. They employed an implicit time stepping scheme with second-order accuracy for discretizes the problem in the time direction, and the radial point interpolation method in the spatial domain. A novel numerical scheme was developed using the direct meshless local Petrov–Galerkin (DMLPG) method for solving complex fractional fourth-order reaction–diffusion equations in [1]. The method combined finite difference and DMLPG techniques for stability and accuracy, showcasing efficiency on varied grid point distributions. A new meshless numerical method for solving 2D time fractional reaction diffusion systems with distributed order on arbitrary domains is studied in [24]. By utilizing Gauss-Legendre quadrature and piecewise parabolic fractional interpolation theory, the approach efficiently handled non-smooth solutions and accurately approximated Caputo fractional derivatives. A local meshfree procedure for simulating the Galilei invariant fractional advection-diffusion equations across one, two, and three-dimensional spaces is investigated in [4]. The method is combined a second-order Crank-Nicolson scheme for time discretization with the second-order weighted and shifted Grünwald difference formula, ensuring stability and convergence. To see the others meshless scheme and their advantages see [6, 7, 13, 17, 18, 20–22, 26] and references therein. In a meshless algorithm, approximations or interpolations play an important role. These approximations are typically employed for discretizing the spatial dimension of a problem. However, when the spatial derivative is of fractional order, applying these approximations becomes challenging. As a result, spatial derivatives are usually considered to be of positive integer order. To address this issue, the fractional derivatives of the shape functions in the method must be computed. One of them is MK interpolation that, which has numerous applications in solving differential equations and in the field of geostatistics. Since the shape functions in this method exhibit the Kronecker delta property, numerous researchers have employed this type of interpolation to address partial differential equations (refer to [5, 12, 14]). The study presented in [15] introduced modifications to the MK shape functions, adapting them for fractional spatial orders with Caputo derivatives, and proposed an efficient meshless approach for solving a space-fractional diffusion model.

Uncorrected Proof

In the present work, we apply the Taylor series expansion to the MK interpolation correlation function and calculate the Riesz fractional derivatives of the MK shape functions to discretize the spatial domain of the primary problem.

The organization of this study is as follows: In section 2, the moving Kriging interpolation method is briefly explained, and the derivative of shape functions for the temporal Riesz fractional order are computed using Taylor expansion. In section 3, the proposed method is constructed on local subdomains, and the discretization of the main problem in the spatial domain is discussed. Section 4 addresses the discretization of the problem in the temporal variable, and a convergence analysis of the method is also provided. To test the accuracy of the method, several examples are presented in section 5. Additionally, a general conclusion is given at the end.

2. The generalization of the MK's shape functions

One of the interpolation methods that has been utilized in meshfree methods is the MK interpolation method. This scheme is commonly employed in the modeling of geostatistical phenomena. Typically, the MK's shape functions are used for discretizing equations in the spatial domain. Most equations considered in this context involve spatial derivatives of integer order. However, when the spatial derivatives of the governing equation are of fractional orders, the use of this technique becomes challenging. In this section, a generalization of the derivatives of MK's shape is presented for cases where the spatial derivative of the problem is of the Riesz type. Assume that Ω is the primary domain of the problem, and points $X_s = \{\mathbf{s}_1, \mathbf{s}_2, \mathbf{s}_3, \dots, \mathbf{s}_N\}$ are a distribution that is sufficiently well-dispersed within this domain. Around these nodes, we construct subdomains with arbitrary shapes [5, 12] (for simplicity, a subinterval in the one-dimensional case and a circle in the two-dimensional case). These subdomains overlap with each other and collectively cover the entire domain. For any desired node $\mathbf{s}_i (1 \leq i \leq N)$, the MK interpolation within its related neighborhood $\Omega_{\mathbf{s}_i}$ is expressed as follows:

$$u(\mathbf{s}) = \sum_{j=1}^{N} \phi_j(\mathbf{s}) u_j = \Phi^T(\mathbf{s}) u, \qquad \mathbf{s} \in \Omega_{\mathbf{s}_i}, \tag{2.1}$$

in which, $u(\mathbf{s})$ represents the interpolated value at $\mathbf{s}$, $\phi_j(\mathbf{s})$ are the shape functions related to the neighboring points, u_j are the values at the neighboring points. In Eq. (2.1) from [13], we have

$$\Phi^T(\mathbf{s}) = p^T(\mathbf{s}) A + \mathbf{r}^T(\mathbf{s}) B, \tag{2.2}$$

in which

$$A = \left(P^T R^{-1} P\right)^{-1} P^T R^{-1}, \qquad B = R^{-1}\left(I - PA\right), \tag{2.3}$$

where I is identity matrix and

$$P = \begin{bmatrix} p_1(\mathbf{s}_1) & \cdots & p_m(\mathbf{s}_1) \\ \cdots & \cdots & \cdots \\ p_1(\mathbf{s}_N) & \cdots & p_m(\mathbf{s}_N) \end{bmatrix}, \qquad R = \begin{bmatrix} \lambda(\mathbf{s}_1, \mathbf{s}_1) & \cdots & \lambda(\mathbf{s}_1, \mathbf{s}_N) \\ \cdots & \cdots & \cdots \\ \lambda(\mathbf{s}_N, \mathbf{s}_1) & \cdots & \lambda(\mathbf{s}_N, \mathbf{s}_N) \end{bmatrix}, \tag{2.4}$$

where $p(\mathbf{s})$ represents a vector containing the complete monomial basis of order m

$$p^T(\mathbf{s}) = [p_1(\mathbf{s}), p_2(\mathbf{s}), \dots, p_m(\mathbf{s})], \tag{2.5}$$

and based on the dimension of governing model, it is given as

$$p^T(\mathbf{s}) = \left[1, x, x^2, x^3, x^4\right], \qquad m = 5,$$

and

$$p^T(\mathbf{s}) = \left[1, x, y, x^2, xy, y^2, x^3, x^2y, xy^2, y^3, x^4, x^3y, x^2y^2, xy^3, y^4\right], \qquad m = 15.$$

Also, we have

$$\mathbf{r}^T(\mathbf{s}) = \left[\lambda(\mathbf{s}, \mathbf{s}_1) \dots \lambda(\mathbf{s}, \mathbf{s}_N)\right], \tag{2.6}$$

where $\lambda(\mathbf{s}, \mathbf{s}_j)$ is referred to as the correlation function and is defined as

$$\lambda_j(\mathbf{s}) = \exp\left(-r_j^2 / c_j^2\right), \tag{2.7}$$

Uncorrected Proof

in which c_j is a constant and it is determined experimentally and r_j is the distance between two points (x, y) and (x_j, y_j). To calculate the partial derivatives of MK's shape functions of a positive integer order with respect to x (or y), the following expression is used:

$$\begin{cases} \dfrac{\partial \phi_i(\mathbf{s})}{\partial x} = \sum_{j=1}^{m} \dfrac{\partial p_i(\mathbf{s})}{\partial x} A_{ji} + \sum_{k=1}^{n_1} \dfrac{\partial r_k(\mathbf{s})}{\partial x} B_{ki}, \\ \dfrac{\partial \phi_i}{\partial y}(\mathbf{s}) = \sum_{j=1}^{m} \dfrac{\partial p_i}{\partial y}(\mathbf{s}) A_{ji} + \sum_{k=1}^{n_1} \dfrac{\partial r_k(\mathbf{s})}{\partial y} r_k B_{ki}. \end{cases} \tag{2.8}$$

To evaluate the Riesz fractional derivatives respect to x or y for MK's shape functions, we begin by determining the Riesz fractional derivatives of x^m and y^m for $m \in \mathbb{Z}^+ \cup \{0\}$ at the interval $[a, b]$. For this, the following expressions are used:

$$x^m = (-x)^m(-1)^m = (-b + b - x)^m(-1)^m = \sum_{k=0}^{m} \binom{m}{k} (-1)^{m+k} b^k (b - x)^{m-k}, \tag{2.9}$$

$$x^m = (x - a + a)^m = \sum_{k=0}^{m} \binom{m}{k} a^k (x - a)^{m-k}. \tag{2.10}$$

So, we have

$${}_{Rz}D_x^{\alpha} x^m = -\frac{1}{2\cos(\frac{\alpha\pi}{2})} \sum_{k=0}^{m} \left(\frac{m!}{k!(m-k+1-\alpha)} a^k (x-a)^{m-k-\alpha} + \frac{m!}{k! m(m-k+1-\alpha)} (-1)^{m+k} b^k (b-x)^{m-k-\alpha} \right), \tag{2.11}$$

and similarly for y^m over the interval $[c, d]$. Additionally, to compute the fractional Riesz case derivative of the correlations function in Eq. (2.7), the following Taylor expansion is employed:

$$\begin{aligned} \lambda_j(\mathbf{s}) = \exp\left(-r_j^2/c_j^2\right) &= \exp\left(-(y - y_j)^2/c_j^2\right) \exp\left(-(x - x_j)^2/c_j^2\right) \\ &= \exp\left(-(y - y_j)^2/c_j^2\right) \sum_{m=0}^{\infty} \frac{f_1^{(m)}(x)}{m!} x^m, \end{aligned} \tag{2.12}$$

in which $f_1(x) = \exp\left(-(x - x_j)^2/c_j^2\right)$. Also, we have

$$\begin{aligned} \lambda_j(\mathbf{s}) = \exp\left(-r_j^2/c_j^2\right) &= \exp\left(-(x - x_j)^2/c_j^2\right) \exp\left(-(y - y_j)^2/c_j^2\right) \\ &= \exp\left(-(x - x_j)^2/c_j^2\right) \sum_{m=0}^{\infty} \frac{f_2^{(m)}(y)}{m!} y^m, \end{aligned} \tag{2.13}$$

in which $f_2(x) = \exp\left(-(y - y_j)^2/c_j^2\right)$. Using relations (2.11),(2.12) and Eq. (2.13), results in:

$$\begin{cases} {}_{Rz}D_x^{\alpha} \phi_i(\mathbf{s}) = \sum_{j=1}^{m} {}_{Rz}D_x^{\alpha} p_i(\mathbf{s}) A_{ji} + \sum_{k=1}^{n_1} {}_{Rz}D_x^{\alpha} \lambda_i(s) B_{ki}, \\ {}_{Rz}D_y^{\alpha} \phi_i(\mathbf{s}) = \sum_{j=1}^{m} {}_{Rz}D_y^{\alpha} p_i(\mathbf{s}) A_{ji} + \sum_{k=1}^{n_1} {}_{Rz}D_y^{\alpha} \lambda_i(\mathbf{s}) B_{ki}. \end{cases} \tag{2.14}$$

We provide a numerical example to test the Riesz fractional derivatives of the shape functions.

Example 2.1. Assume $u(x, y) = x^2 + y^2$, and $\Omega = [0, 1] \times [0, 1]$ so to calculate ${}_{Rz}D_x^{\alpha} u(x, y)$, ${}_{Rz}D_y^{\alpha} u(x, y)$, and ${}_{Rz}\Delta^{\alpha} u(x, y)$, it is sufficient to substitute $m = 2$ into Eq. (2.9).

Table 1 shows the L_2 error between fractional derivative order of $u(x, y)$ and approximation of these fractional derivative. The results in the table indicate that the derivatives of the shape functions exhibit a satisfactory accuracy compared to the fractional derivatives of the mentioned function.

Uncorrected Proof

TABLE 1. The L_2 error between fractional derivative order of $u(x,y)$ and its MK's approximation.

α	$\|\ {}_{Rz}D_x^\alpha U - {}_{Rz}D_x^\alpha \Phi U\|_2$	$\|\ {}_{Rz}D_y^\alpha U - {}_{Rz}D_y^\alpha \Phi U\|_2$	$\|\ {}_{Rz}\Delta^\alpha U - {}_{Rz}\Delta^\alpha \Phi U\|_2$
0.7	$3.8948e-05$	$3.9730e-05$	$5.5706e-05$
0.9	$7.6460e-05$	$7.8111e-05$	$1.0933e-04$
1.3	$1.3313e-04$	$1.3556e-04$	$1.9011e-04$
1.7	$2.0898e-04$	$2.1294e-04$	$2.9854e-04$
1.9	$1.2856e-04$	$1.3094e-04$	$1.8350e-04$

3. The present meshless method

In this section, according to moving Kriging process, a meshfree technique is presented for the spatial discretization of Equation (1.1). This method is essentially a second-type meshless Petrov-Galerkin approach. Instead of constructing the weak form of the equation over the entire problem domain, the weak form is formulated over local subdomains. Let the problem domain Ω contain scattered nodes $\mathbf{s}_j$, $j = 1, 2, \ldots, N$. Instead of evaluating the weak form over the main domain of problem Ω, it is computed within local subdomains. Here, a circular local subdomain is assumed around each node $\mathbf{s}_j$. Consequently, for each point, the following collocation expression is applied within the local subdomain $\Omega_{\mathbf{s}_j}$ associated with $\mathbf{s}_j$:

$$ {}_{CH}D_{\gamma,t}^{\beta} u(\mathbf{s},t) - \Delta^\alpha u(\mathbf{s},t) + u(\mathbf{s},t) = f(\mathbf{s},t), \qquad \mathbf{s} \in \Omega_{\mathbf{s}_j}, \tag{3.1}$$

Assume there are only n_1 points in the subdomain corresponding to $\mathbf{s}_j$. Therefore, the moving Kriging interpolation in this subdomain is expressed as follows:

$$u^h(\mathbf{s}) = \sum_{k=0}^{n_1} \phi_k(\mathbf{s}) \hat{u}_k(t). \qquad \mathbf{s} \in \Omega_{\mathbf{s}_j}, \tag{3.2}$$

and by substituting this relation into Equation (3.1), we arrive at the following expression:

$$\sum_{k=0}^{n_1} \phi_k(\mathbf{s}) \left({}_{CH}D_{\gamma,t}^{\beta} \hat{u}_k(t) \right) - \sum_{k=0}^{n_1} (\Delta^\alpha \phi_k(\mathbf{s}))\, \hat{u}_k(t) + \sum_{k=0}^{n_1} \phi_k(\mathbf{s}) \hat{u}_k(t) = f(\mathbf{s},t), \qquad \mathbf{s} \in \Omega_{\mathbf{s}_j}, \tag{3.3}$$

by repeating this process for all points within the domain, we obtain the following system of matrix equations:

$$\mathbf{C}\left({}_{CH}D_{\gamma,t}^{\beta} U(t) \right) - \mathbf{K}U(t) + \mathbf{C}U(t) = F(t), \tag{3.4}$$

in which

$$\mathbf{C}_{kj} = \phi_k(\mathbf{s}_j) = \begin{cases} 1, & k = j, \\ 0, & k \neq j, \end{cases} \qquad \mathbf{K}_{kj} = \Delta^\alpha \phi_k(\mathbf{s}_j), \qquad \text{and } F_j = f(\mathbf{s}_j, t). \tag{3.5}$$

At this point, the space discretization of the equation is completed. In the following section, the temporal discretization of the problem will be performed, and an analysis of the method will be presented.

4. Semi-discrete scheme

In this section, we will be designated a temporal discretization plan for relation Eq. (3.4). Moreover, the unconditioned stability and convergence analysis for this approach will be proven.

4.1. **Discretization in time variable.** In order to formulate the finite difference algorithm for the fractional problem Eq. (1.1), we define the step size of time $\tau = \frac{T-\gamma}{N_t}$ with $t_k = \gamma + k\tau$ for $\gamma = t_0 < t_1 < \cdots < t_{N_t-1} < t_{N_t} = T$. where

Uncorrected Proof

N_t is a arbitrary positive integer. So, the Caputo-Hadamard fractional derivative $u(\mathbf{s},t)$ is discreted at t_{k+1} for $k=0,1,\ldots,N_t-1$ as follows [11]

$$ {}_{CH}D^{\beta}_{\gamma,t}u(\mathbf{s},t)\Big|_{t=t_k} = \sum_{i=1}^{k+1}\mathscr{C}_{i,k+1}\big(u(\mathbf{s},t_i)-u(\mathbf{s},t_{i-1})\big)+\mathcal{R}_{\beta}, \tag{4.1}$$

in which $\mathcal{R}_{\beta}\leq \mathcal{C}\tau^{2-\beta}$ and

$$ \mathscr{C}_{i,k+1}=\frac{1}{\Gamma(2-\beta)}\frac{1}{\log\frac{t_i}{t_{i-1}}}\left(\left(\log\frac{t_{k+1}}{t_{i-1}}\right)^{1-\beta}-\left(\log\frac{t_{k+1}}{t_i}\right)^{1-\beta}\right). \tag{4.2}$$

Now, the main problem Eq. (1.1) can be approximated at point t_{k+1} as follows

$$ \sum_{i=1}^{k+1}\mathscr{C}_{i,k+1}\big(u(\mathbf{s},t_i)-u(\mathbf{s},t_{i-1})\big)-\Delta^{\alpha}u(\mathbf{s},t_{k+1})+u(\mathbf{s},t_{k+1})=f(\mathbf{s},t_{k+1})+\mathcal{R}_{\beta}, \tag{4.3}$$

or equivalently, we can be written

$$ \big(\mathscr{C}_{k+1,k+1}+1\big)u(\mathbf{s},t_{k+1})-\Delta^{\alpha}u(\mathbf{s},t_{k+1})=\mathscr{C}_{k+1,k+1}u(\mathbf{s},t_k)-\sum_{i=1}^{k}\mathscr{C}_{i,k+1}\big(u(\mathbf{s},t_i)-u(\mathbf{s},t_{i-1})\big)+f(\mathbf{s},t_{k+1})+\mathcal{R}_{\beta}. \tag{4.4}$$

Eliminating the error term $\mathcal{R}_{\beta}$, result in

$$ \big(\mathscr{C}_{k+1,k+1}+1\big)\overline{u}_{k+1}(\mathbf{s})-\Delta^{\alpha}\overline{u}_{k+1}(\mathbf{s})=\mathscr{C}_{k+1,k+1}\overline{u}_{k}(\mathbf{s})-\sum_{i=1}^{k}\mathscr{C}_{i,k+1}\big(\overline{u}_i(\mathbf{s})-\overline{u}_{i-1}(\mathbf{s})\big)+f_{k+1}(\mathbf{s}), \tag{4.5}$$

in which $\overline{u}_{k+1}(\mathbf{s})$ is approximation of $u_{k+1}(\mathbf{s})=u(\mathbf{s},t_{k+1})$.

4.2. **Stability and convergence.** In the present segment, our focus lies on investigating the stability characteristics and convergence rate pertaining to the discretized temporal scheme.

Definition 4.1. The Hilbert space $L_2(\Omega)$ is the space of all measurable functions $w:\Omega\longrightarrow\mathbb{R}$ with the Lebesgue measure $d\mathbf{s}$ on $\mathbb{R}^k$ is defined as

$$ \int_{\Omega}|w(\mathbf{s})|^2 d\mathbf{s}<\infty, \tag{4.6}$$

with the inner product and the following norm, respectively

$$ \langle w,v\rangle=\int_{\Omega}w(\mathbf{s})v(\mathbf{s})d\mathbf{s}, \tag{4.7}$$

and

$$ \|w\|=\left(\int_{\Omega}\big(w(\mathbf{s})\big)^2 d\mathbf{s}\right)^{\frac{1}{2}}. \tag{4.8}$$

Moreover, we consider the real-valued functions space on the bounded domain Ω as follows

$$ \mathcal{H}^1(\Omega)=\{w:\Omega\longrightarrow\mathbb{R}|\ w \text{ and } w_{\mathbf{s}}\in L^2(\Omega)\},\qquad \mathcal{H}^1_0(\Omega)=\{w\in\mathcal{H}^1(\Omega),\ w\big|_{\partial\Omega}=w_{\mathbf{s}}\big|_{\partial\Omega}=0\}. \tag{4.9}$$

Uncorrected Proof

The inner product norm and semi-norm in space $\mathcal{H}^1(\Omega)$ are given as

$$\langle w, v\rangle_{\mathcal{H}^1(\Omega)} = \sum_{0<\alpha\leq 2} \int_\Omega {}^{RL}_{a}D^{\alpha}_{\mathbf{s}} w(\mathbf{s})\ {}^{RL}_{a}D^{\alpha}_{\mathbf{s}} v(\mathbf{s}) d\mathbf{s},$$

$$\|w\|_{\mathcal{H}^1(\Omega)} = \left(\sum_{0<\alpha\leq 2} \| {}^{RL}_{a}D^{\alpha}_{\mathbf{s}} w\| \right)^{\frac{1}{2}},$$

$$|w|_{J^{\alpha}_{R}} = \| {}^{RL}_{a}D^{\alpha}_{\mathbf{s}} w\|.$$

Lemma 4.2. *[15] Assume $w, v \in \mathcal{H}^1_0(\Omega)$. Then, it holds that*

$$\langle {}^{RL}_{a}D^{\alpha}_{x} w,\ {}^{RL}_{x}D^{\alpha}_{b} w\rangle = \cos(\pi\alpha)\| {}^{RL}_{a}D^{\alpha}_{x} w\|^2 = \cos(\pi\alpha)\| {}^{RL}_{x}D^{\alpha}_{b} w\|^2, \qquad \alpha > 0, \tag{4.10}$$

and for $1 < \alpha \leq 2$, we have

$$\langle {}^{RL}_{a}D^{\alpha}_{x} w,\ v\rangle = \langle {}^{RL}_{a}D^{\frac{\alpha}{2}}_{x} w,\ {}^{RL}_{x}D^{\frac{\alpha}{2}}_{b} v\rangle. \tag{4.11}$$

Remark 4.3. For simplification, the relation Eq. (4.1) can be written as follows

$${}_{CH}D^{\beta}_{\gamma,t} u(\mathbf{s},t)\Big|_{t=t_k} = \sum_{i=0}^{k+1} \mathscr{D}_{i,k+1} u(\mathbf{s}, t_i) + \mathcal{R}_{\beta}, \tag{4.12}$$

in which

$$\mathscr{D}_{i,k+1} = \begin{cases} -\mathscr{C}_{1,k+1}, & i = 0, \\ \mathscr{C}_{i,k+1} - \mathscr{C}_{i+1,k+1} & 1 \leq i \leq k, \\ \mathscr{C}_{k+1,k+1}, & i = k+1. \end{cases} \tag{4.13}$$

So, the time-discrete scheme for time variable can obtained as

$$\big(\mathscr{D}_{k+1,k+1} + 1\big) U_{k+1}(\mathbf{s}) - \Delta^{\alpha} U_{k+1}(\mathbf{s}) = f_{k+1}(\mathbf{s}) - \sum_{i=0}^{k} \mathscr{D}_{i,k+1} U_i(\mathbf{s}). \tag{4.14}$$

Theorem 4.4. *The difference scheme Eq. (4.14) for $U_{k+1}(\boldsymbol{s}) \in \mathcal{H}^1_0(\Omega)$ is unconditionally stable.*

Proof. Taking the multiplying both sides of the Equation (4.14) in $U_{k+1}(\mathbf{s})$, results in

$$\big(\mathscr{D}_{k+1,k+1} + 1\big)\|U_{k+1}\|^2 - \langle \Delta^{\alpha} U_{k+1}, U_{k+1}\rangle = \langle f_{k+1}, U_{k+1}\rangle - \sum_{i=0}^{k} \mathscr{D}_{i,k+1} \langle U_i, U_{k+1}\rangle. \tag{4.15}$$

Applying Lemma 4.2, implies that

$$\big(\mathscr{D}_{k+1,k+1} + 1\big)\|U_{k+1}\|^2 - \cos\big(\frac{\pi\alpha}{2}\big)\|\Delta^{\frac{\alpha}{2}} U_{k+1}\|^2 = \langle f_{k+1}, U_{k+1}\rangle - \sum_{i=0}^{k} \mathscr{D}_{i,k+1} \langle U_i, U_{k+1}\rangle. \tag{4.16}$$

Since $\cos\big(\frac{\pi\alpha}{2}\big)\|\Delta^{\frac{\alpha}{2}} U_{k+1}\|^2 \leq 0$ for $1 < \alpha \leq 2$ and using Cauchy–Schwarz inequality, we have

$$\begin{aligned} \big(\mathscr{D}_{k+1,k+1} + 1\big)\|U_{k+1}\|^2 &\leq \langle f_{k+1}, U_{k+1}\rangle - \sum_{i=0}^{k} \mathscr{D}_{i,k+1} \langle U_i, U_{k+1}\rangle \\ &\leq \|f_{k+1}\|\|U_{k+1}\| - \sum_{i=0}^{k} \mathscr{D}_{i,k+1} \|U_i\|\|U_{k+1}\| \\ &\leq \|f_{k+1}\|\|U_{k+1}\| + \sum_{i=0}^{k} |\mathscr{D}_{i,k+1}|\|U_i\|\|U_{k+1}\|. \end{aligned} \tag{4.17}$$

Uncorrected Proof

We can get the following inequality by the relation Eq. (4.17) as

$$\|U_{k+1}\| \leq \frac{1}{\mathscr{D}_{k+1,k+1}+1}\|f_{k+1}\| + \frac{|\mathscr{D}_{k+1,k+1}|}{\mathscr{D}_{k+1,k+1}+1}\sum_{i=0}^{k}\|U_i\| \tag{4.18}$$
$$\leq \frac{1}{\mathscr{D}_{k+1,k+1}+1}\|f_{k+1}\| + \sum_{i=0}^{k}\|U_i\|.$$

By simplification the above relation, we can write

$$\|U_{N_t}\| \leq N_t\mathfrak{C}\max_{\mathbf{s}\in\Omega}|f_{N_t}(\mathbf{s})| + N_t\|U_0\|, \tag{4.19}$$

in which $\mathfrak{C} > 0$ is constant and with multiplying τ on both sides of the previous relation yields

$$\tau\|U_{N_t}\| \leq \tau N_t\mathfrak{C}\max_{\mathbf{s}\in\Omega}|f_{N_t}(\mathbf{s})| + \tau N_t\|U_0\|$$
$$\leq \big(T-\mathfrak{r}\big)\mathfrak{C}\max_{\mathbf{s}\in\Omega}|f_{N_t}(\mathbf{s})| + \big(T-\mathfrak{r}\big)\|U_0\|. \tag{4.20}$$

Finally, one obtains

$$\|U_{N_t}\| \leq \mathfrak{C}^{\star}\Big(\max_{\mathbf{s}\in\Omega}|f_{N_t}(\mathbf{s})| + \|U_0\|\Big), \tag{4.21}$$

where $\mathfrak{C}^{\star}$ is positive constant and $\|U_0\| = \|u_0\|$. □

Theorem 4.5. *If u_{k+1} and $U_{k+1} \in \mathcal{H}_0^1(\Omega)$ be the true and numerical solutions of finite difference algorithm Eq. (4.14). Then, scheme Eq. (4.14) is convergent with time convergence order $\mathcal{O}(\tau)$.*

Proof. By subtracting the semi-discrete scheme Eq. (4.14) for exact and approximate solutions and putting $\mathfrak{e}_{k+1} = u_{k+1} - U_{k+1}$ such that $\mathfrak{e}_0 = 0$, we have

$$\big(\mathscr{D}_{k+1,k+1}+1\big)\mathfrak{e}_{k+1}(\mathbf{s}) - \Delta^{\alpha}\mathfrak{e}_{k+1}(\mathbf{s}) = -\sum_{i=0}^{k}\mathscr{D}_{i,k+1}\mathfrak{e}_i(\mathbf{s}) + \mathcal{R}_{\beta}. \tag{4.22}$$

From the inner product Eq. (4.22) in $\mathfrak{e}_{k+1} \in \mathcal{H}_0^1(\Omega)$, arrives at

$$\big(\mathscr{D}_{k+1,k+1}+1\big)\|\mathfrak{e}_{k+1}\|^2 - \langle\Delta^{\alpha}\mathfrak{e}_{k+1},\mathfrak{e}_{k+1}\rangle = -\sum_{i=0}^{k}\mathscr{D}_{i,k+1}\langle\mathfrak{e}_i,\mathfrak{e}_{k+1}\rangle + \langle\mathcal{R}_{\beta},\mathfrak{e}_{k+1}\rangle. \tag{4.23}$$

With the same technique as in Theorem 4.4 and $\mathscr{D}_{k+1,k+1} = \mathscr{C}_{k+1,k+1} = \dfrac{1}{\Gamma(2-\beta)}\Big(\log\dfrac{t_{k+1}}{t_k}\Big)^{-\beta} \leq \tau^{-\beta}$, we can conclude

$$\|\mathfrak{e}_{k+1}\| \leq \frac{1}{\mathscr{D}_{k+1,k+1}+1}\mathcal{R}_{\beta} + \sum_{i=0}^{k}\|\mathfrak{e}_i\| \leq \mathcal{C}\tau^2 + \sum_{i=0}^{k}\|\mathfrak{e}_i\|, \qquad \mathcal{C} > 0, \tag{4.24}$$

or equivalently

$$\|\mathfrak{e}_{N_t}\| \leq N_t\mathcal{C}\tau^2 + N_t\|\mathfrak{e}_0\| = N_t\mathcal{C}\tau^2. \tag{4.25}$$

Applying the scalar multiplication recent relation in τ, we can get the following inequality

$$\tau\|\mathfrak{e}_{N_t}\| \leq \tau N_t\mathcal{C}\tau^2 = \big(T-\mathfrak{r}\big)\mathcal{C}\tau^2. \tag{4.26}$$

Finally, the proof is concluded by dividing both sides of the relation Eq. (4.26) by the factor τ. □

Uncorrected Proof

5. Numerical Experiments

In this section, numerical examples are presented to test the proposed method. The tools utilized here are the following norms, the definitions of which are provided below:

$$L_2 = \sqrt{\sum_{i=1}^{N} \left(u(\mathbf{s}_i) - u^h(\mathbf{s}_i)\right)^2}, \qquad L_\infty = \max_{\mathbf{s}_i \in \Omega} \left|u(\mathbf{s}_i) - u^h(\mathbf{s}_i)\right|, \tag{5.1}$$

where $u(\mathbf{s}_i)$ and $u^h(\mathbf{s}_i)$ represent the exact and numerical solutions at the node $\mathbf{s}_i$, respectively to show validity of the method, the time variable order is calculated as

$$C - \text{order} = \frac{\log\left(\frac{\mathcal{E}_1}{\mathcal{E}_2}\right)}{\log\left(\frac{\tau_1}{\tau_2}\right)}, \tag{5.2}$$

in which $\mathcal{E}_1$ and $\mathcal{E}_2$ are errors related to τ_1 and τ_2, respectively. The subdomains are assumed to be circular in shape. There is no specific method for determining the constant coefficient c_j, it is typically obtained through trial and error. In this work, we set it to $c_j = 0.8$.

Example 5.1. Assume the following Caputo–Hadamard time, Caputo-space Riesz fractional reaction–diffusion equation

$${}_{CH}D^{\beta}_{1,t} u(\mathbf{s},t) - \Delta^{\alpha} u(\mathbf{s},t) + u(\mathbf{s},t) = f(\mathbf{s},t), \quad \mathbf{s} = (x,y) \in \Omega_1, \quad 1 \le t \le T, \tag{5.3}$$

with the following Dirichlet boundary conditions

$$u(\mathbf{s},t) = (\log t)^2 (x^2 + y^2), \qquad (x,y) \in \partial\Omega_1, \tag{5.4}$$

and homogeneous initial conditions. Here, the exact solution is $u(\mathbf{s},t) = (\log t)^2(x^2+y^2)$. The force term f can be derived from the exact solution as follows

$$\begin{aligned} f(\mathbf{s},t) = {} & \frac{2}{\Gamma(3-\beta)} (\log t)^{3-\beta} (x^2+y^2) \\ & - \frac{(\log t)^2}{\cos(\alpha\pi/2)} \left(\frac{1}{\Gamma(3-\alpha)} x^{2-\alpha} + \frac{1}{\Gamma(3-\alpha)} (1-x)^{2-\alpha} - \frac{1}{\Gamma(2-\alpha)} (1-x)^{1-\alpha} \right. \\ & + \frac{1}{2\Gamma(1-\alpha)} (1-x)^{-\alpha} + \frac{1}{\Gamma(3-\alpha)} y^{2-\alpha} + \frac{1}{\Gamma(3-\alpha)} (1-y)^{2-\alpha} \\ & \left. - \frac{1}{\Gamma(2-\alpha)} (1-y)^{1-\alpha} + \frac{1}{2\Gamma(1-\alpha)} (1-y)^{-\alpha} \right) \\ & + \frac{(\log t)^2}{2\cos(\alpha\pi/2)\Gamma(1-\alpha)} \left[(x^{-\alpha} + (1-x)^{-\alpha}) y^2 + (y^{-\alpha} + (1-y)^{-\alpha}) x^2 \right] \\ & + (\log t)^2 (x^2+y^2). \end{aligned}$$

The numerical solution of this example has been performed using the present numerical method in the domain Ω_1 with 121 uniformly distributed points. Table 2 presents the results for different spatial and temporal orders at large final times. The time step used here is $\tau = 0.005$. To enforce Dirichlet boundary conditions, the Kronecker delta property of the shape functions has been employed. The results indicate the satisfactory accuracy of the present method for the numerical solution of this equation.

Table 3 reports the L_∞ error between exact solution and numerical method. The Caputo-Hadamard time and Caputo-space Riesz fractional orders are $\beta = 0.6, 0.8$ and $\alpha = 1.2$ respectively. Based on this table, the error decreases from the top to the bottom. Additionally, the temporal order of this method is demonstrated here. The results indicate that the temporal order is approximately one, which confirms the findings of Theorem 4.5.

Uncorrected Proof

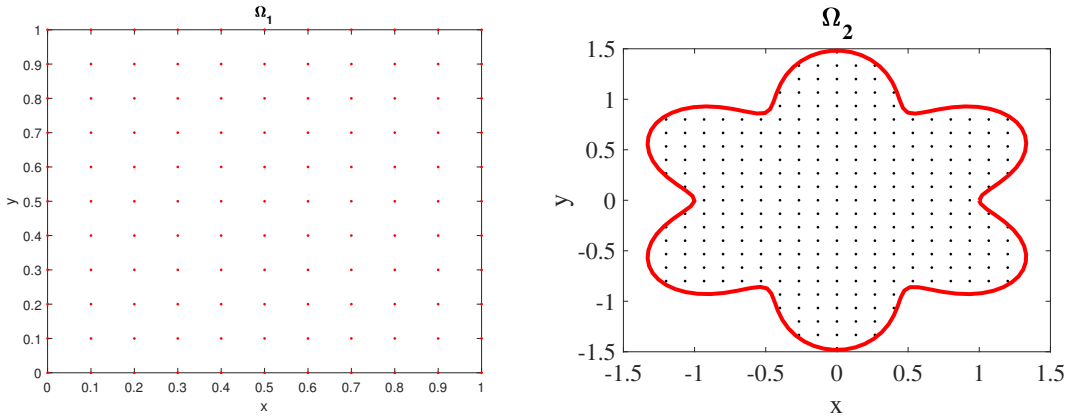

FIGURE 1. The global domains Ω_1(consisting of 121 irregular) and Ω_2 for Example 5.1, 5.2, and 5.3.

TABLE 2. The computations contain L_∞ and L_2 errors at various Caputo–Hadamard time and spatial Riesz fractional orders at $\tau = 0.005$ for Example 5.1.

		$T=2$		$T=5$		$T=8$	
β	α	L_∞	L_2	L_∞	L_2	L_∞	L_2
0.4	1.2	$1.0443e-05$	$4.9966e-05$	$7.3305e-05$	$3.5073e-04$	$1.3012e-04$	$6.2254e-04$
	1.5	$5.7981e-06$	$2.7776e-05$	$4.0920e-05$	$1.9604e-04$	$7.3298e-05$	$3.5116e-04$
	1.8	$5.6871e-06$	$2.7285e-05$	$3.9924e-05$	$1.9154e-04$	$7.2481e-05$	$3.4778e-04$
0.7	1.2	$2.3984e-05$	$1.1475e-04$	$1.2529e-04$	$5.9946e-04$	$2.0006e-04$	$9.5718e-04$
	1.5	$1.3525e-05$	$6.4798e-05$	$7.0124e-05$	$3.3595e-04$	$1.1377e-04$	$5.4514e-04$
	1.8	$1.3301e-05$	$6.3818e-05$	$6.9181e-05$	$3.3194e-04$	$1.1097e-04$	$5.3248e-04$
0.9	1.2	$3.6044e-05$	$1.7245e-04$	$1.5145e-04$	$7.2459e-04$	$2.2420e-04$	$1.0727e-03$
	1.5	$2.0392e-05$	$9.7702e-05$	$8.6023e-05$	$4.1217e-04$	$1.2641e-04$	$6.0567e-04$
	1.8	$1.9973e-05$	$9.5839e-05$	$8.3647e-05$	$4.0135e-04$	$1.2314e-04$	$5.9086e-04$

TABLE 3. The computations contain L_∞ errors and $C-$order of proposed technique at $T = 2$ for Example 5.1.

τ	L_∞	$C-$order	L_∞	$C-$order	CPU
0.01	$3.7429e-05$	–	$5.9070e-05$	–	1.08
0.01/2	$1.8825e-05$	0.9915	$2.9701e-05$	0.9919	2.55
0.01/4	$9.3983e-06$	1.0022	$1.4869e-05$	0.9982	8.06
0.01/8	$4.7287e-06$	0.9910	$7.4490e-06$	0.9972	30.84

Uncorrected Proof

Figure 2 shows the absolute error and the numerical solution applying the proposed scheme. The numerical results demonstrate that the present technique provides a good and appropriate numerical approximation for solving Example 5.1.

Example 5.2. In this case, we assume Equation (1.1) in the following form:

$$ {}_{CH}D^{\beta}_{1,t}u(\mathbf{s},t) - \Delta^{\alpha}u(\mathbf{s},t) + u(\mathbf{s},t) = f(\mathbf{s},t), \quad \mathbf{s} = (x,y) \in \Omega_1, \qquad 1 \le t \le T. \tag{5.5} $$

The overall domain of the problem is assumed to be the same as the domain in Example 5.1. The initial and boundary conditions are considered as follows:

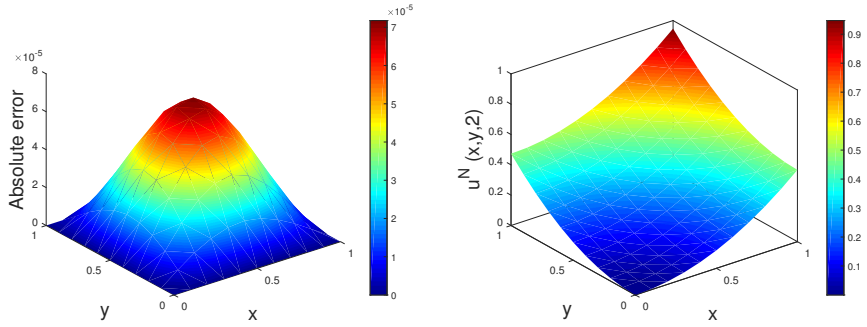

FIGURE 2. The numerical solution and absolute error for Example 5.1.

TABLE 4. The computations contain L_∞ and L_2 errors at various Caputo–Hadamard time and spatial Riesz fractional orders at $\tau = 0.005$ for Example 5.2.

		$T = 1.5$		$T = 2$		$T = 4$	
β	α	L_∞	L_2	L_∞	L_2	L_∞	L_2
0.4	1.1	$2.0151e-04$	$1.6525e-03$	$1.1208e-03$	$9.0864e-03$	$5.0600e-03$	$4.2726e-02$
	1.5	$3.3403e-04$	$3.3314e-03$	$5.5882e-04$	$4.5915e-03$	$1.8429e-03$	$1.5719e-02$
	1.8	$1.9173e-04$	$1.4776e-03$	$5.0309e-04$	$4.0048e-03$	$2.1430e-03$	$2.1232e-02$
0.7	1.1	$2.1450e-04$	$1.7859e-03$	$9.8935e-04$	$7.5172e-03$	$4.2338e-03$	$3.1156e-02$
	1.5	$1.5295e-04$	$1.5647e-03$	$1.3206e-03$	$9.6061e-03$	$3.6583e-03$	$3.0409e-02$
	1.8	$3.2166e-04$	$2.6092e-03$	$5.3936e-04$	$4.1798e-03$	$1.9059e-03$	$1.9112e-02$
0.9	1.1	$2.9754e-04$	$2.0096e-03$	$6.3250e-04$	$5.3015e-03$	$3.2834e-03$	$2.2843e-02$
	1.5	$3.7672e-04$	$3.3775e-03$	$5.7930e-04$	$5.7764e-03$	$3.3365e-03$	$2.7330e-02$
	1.8	$3.4513e-04$	$2.8646e-03$	$1.0630e-03$	$8.9658e-03$	$5.1191e-03$	$4.0172e-02$

$$u(\mathbf{s},1) = 0, \qquad \text{Initial condition}$$

$$\begin{cases} u(x,0,t) = 0, & u(x,1,t) = (\log t)^2 \sin(x)\sin 1, \\ u(0,y,t) = 0, & u(1,y,t) = (\log t)^2 \sin(1)\sin y, \end{cases} \qquad \text{Boundary conditions}$$

The exact solution is $u(x,y,t) = (\log t)^2 \sin(x)\sin(y)$ By using the Taylor expression of $\sin(x)\sin(y)$ and relations (1.4), (2.11), we can calculate the force term $f(\mathbf{s},t)$ for this example. The results for this example using the present method are shown in Table 4. Here, 441 points with uniform distribution are applied within the domain. The time step for this example is $\tau = 0.005$, the final times are $T = 1.5, 2, 4$. Different cases for various fractional orders are presented in this table, demonstrating the high accuracy of the MK shape functions for the numerical solution of this example. In Figure 3, the numerical solution and absolute error are presented for different fractional orders of time and space at various final times. Based on this figure, the numerical solutions done with the propose method provide a good approximation of the true solution.

Example 5.3. In this example, we assume Equation (1.1) with the following Dirichlet boundary and initial conditions:

$$u(\mathbf{s},2) = 0, \qquad \text{Initial condition},$$

$$u(\mathbf{s},t) = (\log(t/2))^6 \exp(x+y), \qquad \mathbf{s} \in \partial\Omega_2 \quad 2 \le t \le T, \quad \text{Boundary conditions},$$

in which $t \in [2,T]$. The exact solution is $u(\mathbf{s},t) = (\log(t/2))^6 \exp(x+y)$. To calculate the right hand side function $f(\mathrm{s},t)$ we use the Taylor expression of $\exp(x)\exp(y)$ and relations (1.4), (2.11).

Uncorrected Proof

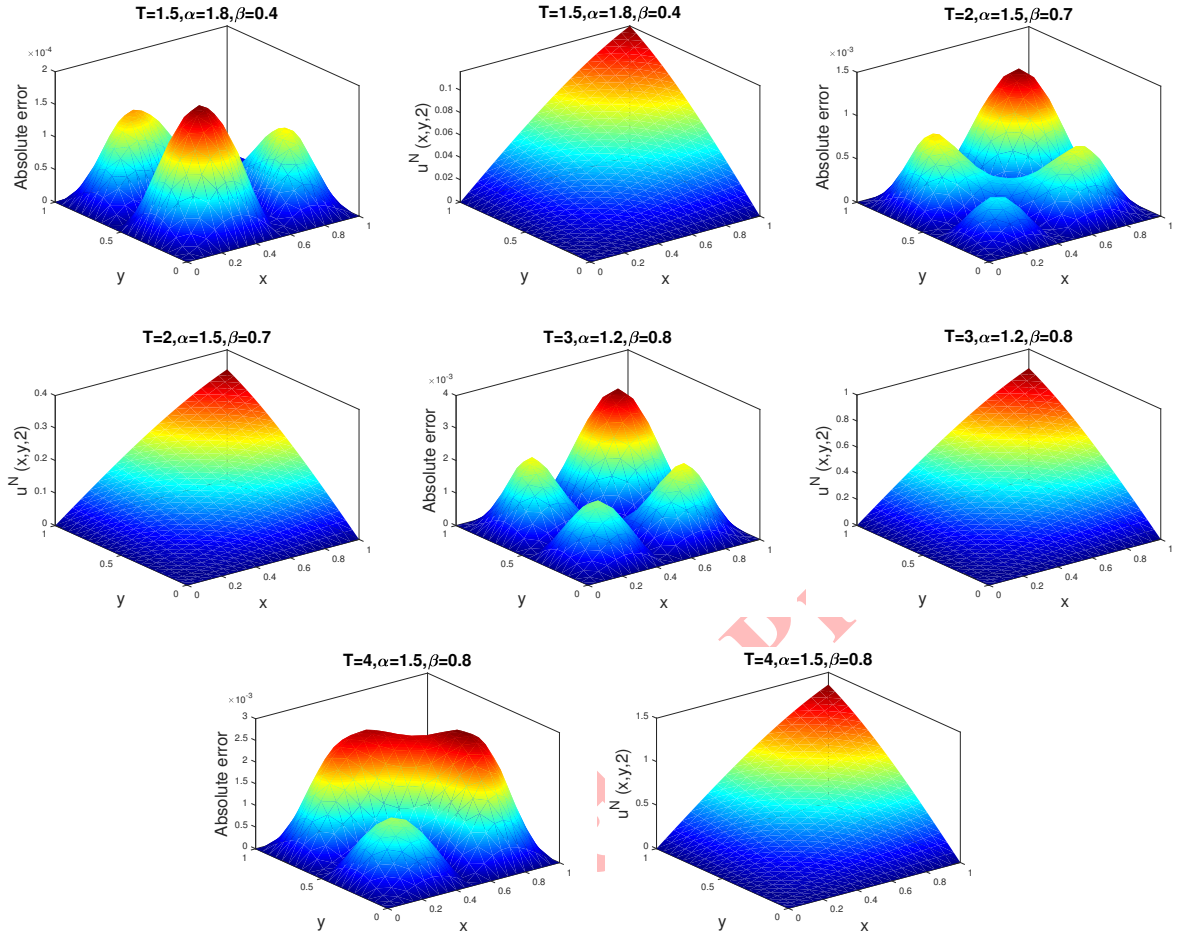

FIGURE 3. The numerical solution and absolute error for different case of T, α, and β for Example 5.2.

One notable feature of mesh-free methods is their flexibility in handling irregular domains. Here, we take the domain in the shape of Ω_2. The polar form of the boundary of this global domain is expressed as follows

$$\left\{(x,y) \in \mathbb{R}^2 : x = r\cos(\theta), y = r\sin(\theta), \quad \theta \in [0, 2\pi], \qquad r = 1 + 0.5\tanh(2\sin 3t)\sin 3t\right\}.$$

In Table 5, results analogous to those in the previous examples are presented for different cases related to this example. The results in Table 5 demonstrate the accuracy of the method for solving Equation (1.1) within the irregular domain Ω_2. In this example, 121 boundary points and 289 interior points have been employed. This example illustrates that the method remains effective in an irregular domain without requiring a grid. To apply the boundary conditions, we utilize the Kronecker delta property of the shape functions. Observing the domain shape, we note that it is generally contained within the rectangle $[-1.5\ 1.5] \times [-1.5\ 1.5]$. Therefore, in this example, the fractional-order derivative is computed in the spatial dimension as follows:

$$\begin{cases} (-\Delta_x)^\alpha u(\mathbf{s},t) = -\frac{1}{2\cos(\frac{\alpha\pi}{2})}[{}^{RL}_{-1.5}D^\alpha_x u(\mathbf{s},t) + {}^{RL}_{x}D^\alpha_{1.5} u(\mathbf{s},t)], \\ (-\Delta_y)^\alpha u(\mathbf{s},t) = -\frac{1}{2\cos(\frac{\alpha\pi}{2})}[{}^{RL}_{-1.5}D^\alpha_y u(\mathbf{s},t) + {}^{RL}_{y}D^\alpha_{1.5} u(\mathbf{s},t)]. \end{cases}$$

In Figure 4, the absolute error between the exact solutions and the solutions obtained using the present method over

Uncor

TABLE 5. The computations contain L_∞ and L_2 errors at various Caputo–Hadamard time and spatial Riesz fractional orders at $\tau = 0.005$ for Example 5.3.

		$T = 2.5$		3		$T = 4$	
β	α	L_∞	L_2	L_∞	L_2	L_∞	L_2
0.4	1.1	$6.6773e-04$	$3.1739e-03$	$1.1501e-03$	$5.4501e-03$	$1.7066e-03$	$8.1187e-03$
	1.5	$5.1226e-04$	$2.5145e-03$	$9.7109e-04$	$4.8963e-03$	$1.4517e-03$	$7.1576e-03$
	1.8	$6.7608e-04$	$3.1978e-03$	$1.0103e-03$	$5.2734e-03$	$1.5171e-03$	$7.6178e-03$
0.7	1.1	$6.7726e-04$	$3.2383e-03$	$1.1616e-03$	$5.5107e-03$	$1.5870e-03$	$7.4600e-03$
	1.5	$5.8486e-04$	$2.9038e-03$	$9.0609e-04$	$4.5517e-03$	$1.2714e-03$	$6.3378e-03$
	1.8	$6.2507e-04$	$3.0255e-03$	$9.0433e-04$	$5.0004e-03$	$1.6104e-03$	$7.9801e-03$
0.9	1.1	$6.7764e-04$	$3.2394e-03$	$1.2140e-03$	$5.8205e-03$	$1.7410e-03$	$8.3284e-03$
	1.5	$5.0131e-04$	$2.5490e-03$	$9.5797e-04$	$4.8097e-03$	$1.2716e-03$	$6.2650e-03$
	1.8	$5.9995e-04$	$3.0704e-03$	$9.7138e-04$	$5.0989e-03$	$1.6442e-03$	$7.8422e-03$

the irregular domain Ω_2 is shown under various cases of T, α and β . As illustrated, the present method demonstrates high accuracy across irregular domains, indicating its robustness and reliability for handling complex geometries.

Table 5 and Figure 4 illustrate the adequate accuracy of this method for solving this example. The results confirm that the proposed approach is effective in achieving reliable solutions, even in cases involving complex domain geometries.

6. Conclusion

This paper presented a robust meshless technique for addressing the Caputo–Hadamard time and Riesz fractional reaction–diffusion equation. Unlike conventional meshless methods, such as those using MK interpolation to calculate shape functions and their integer-order spatial derivatives for equation discretization, this study introduced an enhancement. Specifically, it refined the shape function derivatives to accommodate arbitrary fractional orders $1 < \alpha < 2$ by leveraging the Taylor series expansion of the MK interpolation's correlation function, treating them as Riesz fractional derivatives. For the time component, a finite difference approach was utilized, offering the benefits of unconditional stability and a convergence rate of $O(\tau)$. This method converted the main problem into a system of linear equations. Several examples were presented to assess the accuracy and efficiency of the proposed technique in regular and irregular domains.

Uncorrected Proof

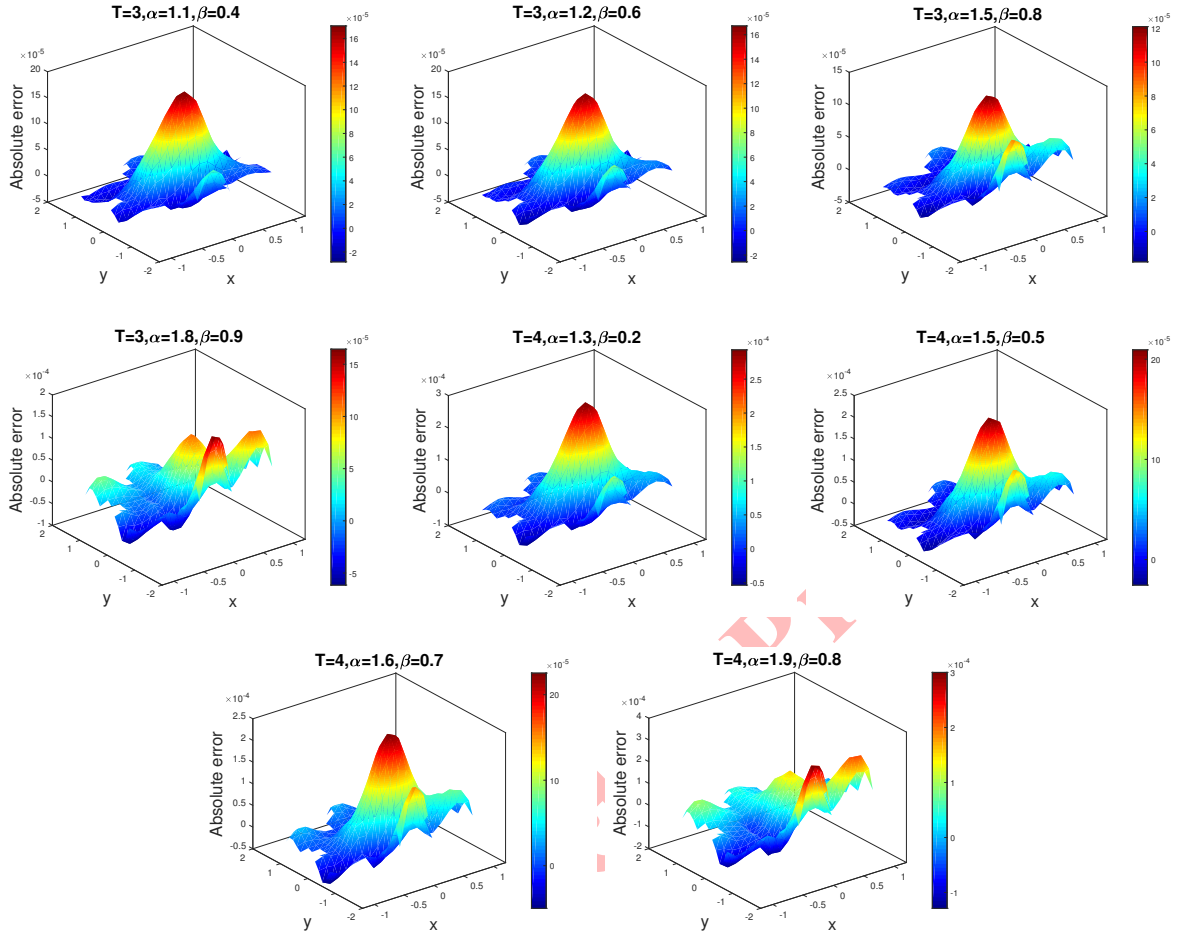

FIGURE 4. The absolute error for different cases at T, α, and β, for Example 5.3.

Uncor

REFERENCES

[1] M. Abbaszadeh and M. Dehghan, *Direct Meshless Local Petrov–Galerkin (DMLPG) method for time-fractional fourth-order reaction–diffusion problem on complex domains*, Computers & Mathematics with Applications, *79*(3) (2020), 876–888.

[2] B. Ahmad, A. Alsaedi, S. K. Ntouyas, and J. Tariboon, *Hadamard-type fractional differential equations, inclusions and inequalities*, Springer, 2017.

[3] B. Baeumer, M. Kovács, and Mark M Meerschaert, *Numerical solutions for fractional reaction–diffusion equations*, Computers & Mathematics with Applications, *55*(10) (2008), 2212–2226.

[4] N. Biranvand and A. Ebrahimijahan, *Numerical study of the multi-dimensional Galilei invariant fractional advection–diffusion equation using direct mesh-less local petrov–galerkin method*, Engineering Analysis with Boundary Elements, *167* (2024), 105910.

[5] L. Chen and K. M. Liew, *A local Petrov-Galerkin approach with moving kriging interpolation for solving transient heat conduction problems*, Computational Mechanics, *47*(4) (2011), 455–467.

[6] M. Dehghan and A. Shokri, *Numerical solution of the nonlinear Klein–Gordon equation using radial basis functions*, Journal of Computational and Applied Mathematics, *230*(2) (2009), 400–410.

[7] M. Dehghan and A. Nikpour, *Numerical solution of the system of second-order boundary value problems using the local radial basis functions based differential quadrature collocation method*, Applied Mathematical Modelling, *37*(18-19) (2013), 8578–8599.
[8] M. Dehghan, M. Abbaszadeh, and A. Mohebbi, *Analysis of a meshless method for the time fractional diffusion-wave equation*, Numerical algorithms, *73* (2016), 445–476.
[9] E. Fan, C. Li, and Zh. Li, *Numerical approaches to Caputo–Hadamard fractional derivatives with applications to long-term integration of fractional differential systems*, Communications in Nonlinear Science and Numerical Simulation, *106* (2022), 106096.
[10] H. R. Ghehsareh, A. Zaghian, and S. M. Zabetzadeh, *An efficient meshless computational technique to simulate nonlinear anomalous reaction–diffusion process in two-dimensional space*, Nonlinear Dynamics, *96* (2019), 1191–1211.
[11] M. Gohar, C. Li, and Z. Li, *Finite difference methods for Caputo–Hadamard fractional differential equations*, Mediterranean Journal of Mathematics, *17*(6) (2020), 194.
[12] L. Gu, *Moving Kriging interpolation and element-free Galerkin method*, International journal for numerical methods in engineering, *56*(1) (2003), 1–11.
[13] A. Habibirad, E. Hesameddini, and A. Taleei, *An efficient meshless method for solving multi-dimensional nonlinear Schrödinger equation*, Iranian Journal of Science and Technology, Transactions A: Science, *44*(3) (2020), 749–761.
[14] A. Habibirad, H. Azin, and E. Hesameddini, *A capable numerical meshless scheme for solving distributed order time-fractional reaction–diffusion equation*, Chaos, Solitons & Fractals, *166* (2023), 112931.
[15] A. Habibirad, O. Baghani, E. Hesameddini, M. Heydari, and H. Azin, *A meshless method based on the modified moving Kriging interpolation for numerical solution of space-fractional diffusion equation*, Engineering Analysis with Boundary Elements, *163* (2024), 1–11.
[16] J. Hadamard, *Essai sur l'étude des fonctions données par leur développement de taylor*. Journal de mathématiques pures et appliquées, *8* (1892), 101–186.
[17] M. K. Kadalbajoo, A. Kumar, and L. P. Tripathi, *A radial basis function based implicit–explicit method for option pricing under jump-diffusion models*, Applied Numerical Mathematics, *110* (2016), 159–173.
[18] M. K. Kadalbajoo, A. Kumar, and L. P. Tripathi, *Radial-basis-function-based finite difference operator splitting method for pricing american options*, International Journal of Computer Mathematics, *95*(11) (2018), 2343–2359.
[19] N. Kedia, A. A. Alikhanov, and V. . Singh, *Higher order computational approach for generalized time-fractional diffusion equation*, Communications on Applied Mathematics and Computation, (2024), 1–23.
[20] A. Kumar, A. Bhardwaj, and B. V. R. Kumar, *A meshless local collocation method for time fractional diffusion wave equation*, Computers & Mathematics with Applications, *78*(6) (2019), 1851–1861.
[21] A. Kumar, A. Bhardwaj, and S. Dubey, *A local meshless method to approximate the time-fractional telegraph equation*, Engineering with Computers, (2020), 1–16.
[22] A. Kumar and A. Bhardwaj, *A local meshless method for time fractional nonlinear diffusion wave equation*, Numerical Algorithms, (2020), 1–24.
[23] K. Kumar, A. K. Pandey, and R. K. Pandey, *High order numerical scheme for generalized fractional diffusion equations*, International Journal of Applied and Computational Mathematics, *10*(3) (2024), 105.
[24] L. Li, Zh. Chen, H. Du, W. Jiang, and B. Zhang, *A meshless approach based on fractional interpolation theory and improved neural network bases for solving non-smooth solution of 2d fractional reaction–diffusion equation with distributed order*, Communications in Nonlinear Science and Numerical Simulation, *138* (2024), 108245.
[25] C. Ou, D. Cen, Z. Wang, and S. Vong, *Fitted schemes for Caputo-Hadamard fractional differential equations*. Numerical Algorithms, (2023), 1–30.
[26] A. Shokri and A. Habibirad, *A moving Kriging-based MLPG method for nonlinear Klein–Gordon equation*, Mathematical Methods in the Applied Sciences, *39*(18) (2016), 5381–5394.
[27] Y. Zhang and H. Ding, *Finite difference method for solving the time fractional diffusion equation*, Asia Simulation Conference, (2012), 115–123.

Uncorrected Proof